東北大学機関リポジトリ
TOUR
Tohoku University Repository
東北大学

Local structures in the superionic conductor Y3+-doped Ce02 studied using site-selective spectroscopy

著者	湯上　浩雄
journal or publication title	Physical review. B
volume	B 44
number	10
page range	4862-4871
year	1991
URL	http://hdl.handle.net/10097/35545

doi: 10.1103/PhysRevB.44.4862

Local structures in the superionic conductor Y^{3+}-doped CeO_2 studied using site-selective spectroscopy

H. Yugami, A. Nakajima, and M. Ishigame
Research Institute of Scientific Measurements, Tohoku University, Katahira 2-1, Aoba-ku, Sendai 980, Japan

T. Suemoto
The Institute for Solid State Physics, The University of Tokyo, Roppongi 7-22-1, Minato-ku, Tokyo 106, Japan
(Received 15 October 1990)

Luminescence spectra of Eu^{3+} ions in Y^{3+}-doped CeO_2 crystals are measured as a function of excitation wavelength for samples of various Y^{3+} concentrations. Eu^{3+} ions, which partially substitute for Y^{3+} ions, act as a structural probe. It is found that six different sites of Eu^{3+} ions exist in this material. A local-structure model is proposed for these sites and experimental results are well explained with this model. The dopant-concentration dependence of the luminescence spectra reveals that the defect center of the oxygen vacancy associated with one Y^{3+} ion is closely related to the ionic conducting mechanism in this sytem.

I. INTRODUCTION

Some of the oxides having fluorite structure (e.g., CeO_2, ZrO_2, etc.) exhibit high ionic conductivity at elevated temperature by the addition of various divalent (Ca^{2+} and Mg^{2+} etc.) or trivalent (Y^{3+}, Yb^{3+}, etc.) cations in a wide range of concentration. In these electrolytes the current is carried by oxygen vacancies, which are introduced to compensate the lower charge of the dopant cations.[1] In particular, yttrium-stabilized zirconia (YSZ) has been most widely used as a solid electrolyte material for oxygen sensors, fuel cells, etc.[2]

Since ionic conduction arises from hopping of oxygen ions through anion vacant sites, a monotonic increase of the ionic conductivity is expected with increasing concentration of the dopant cations. The ionic conductivity, however, goes through a maximum with increasing dopant concentrations.[1,3] This is a common feature in many fluorite-type oxygen-ion conductors. The origins of this behavior of ionic conductivity have been studied by many workers mainly on stabilized zirconia systems with various experimental techniques.[4–7] They suggested that the decrease of ionic conductivity at high dopant concentration may be attributed to clustering, ordering, or formation of a second phase.

The Y_2O_3-doped CeO_2 system is a favored system for investigating such defect structures in the very dilute range of dopant concentrations, because pure CeO_2 has fluorite structure. This situation is in contrast to the case of ZrO_2, which has a tetragonal crystal structure in the dilute range of dopant concentrations.

In contrast to the case of YSZ, the relationship between the local structures and the ionic conductivity for the doped CeO_2 system has not been clarified to date. Ionic conductivity[8] and dielectric relaxation[9] of the Y^{3+}-doped CeO_2 system were studied in detail by Nowick and co-workers. They found that the ionic conductivity rises sharply, giving a maximum at about 4 mol % Y_2O_3 and the activation energy gives a minimum at about 4 mol %. The decrease of the activation energy of the ionic motion in the dilute range of dopant concentration is attributed to the electrostatic interaction between a (V_O,Y) cluster and a Y defect, where V_O represents the oxygen vacancy.

Neutron-scattering measurement were performed by Fender[10] and Anderson *et al.*[11] Fender proposed a complex cluster, which consisted of two oxygen vacancies and three or four Y^{3+} ions, in 5 mol % Y_2O_3-doped CeO_2. Anderson *et al.*, however, stated that the diffuse neutron-scattering data can be represented by a more simple cluster, i.e., the single-vacancy model compensated by one or two Y^{3+} ions for 6 mol % Y_2O_3-doped CeO_2. However, concerning the local structures at higher dopant concentrations, only few qualitative discussions were presented. A systematic investigation over a wide dopant-concentration range is necessary in order to understand the role of local structures on the ionic transport properties of this material.

The purpose of this study is to investigate the local structures surrounding the trivalent impurity metal ion in the Y_2O_3-doped CeO_2 system, and to clarify the relationship between the local structures and the ionic conductivity by using site-selective spectroscopy. This spectroscopic technique is suitable for studying optical properties on disordered system such as amorphous and glass materials,[12] because the inhomogeneous broadening of luminescence bands can be eliminated. The superionic conducting material is a disordered system, because the mobile-ion sublattice is usually highly disordered. Therefore, site-selective spectroscopy is expected to be a very powerful technique to investigate the properties of superionic conductors.

A luminescence study on the CeO_2 system has been reported only by Linares,[13] to our knowledge. He excited Eu^{3+}-doped CeO_2 crystals with x rays and observed visible luminescence spectra of Eu^{3+} ions at room temperature.

 ©1991 The American Physical Society

In our study small amounts of Eu^{3+} ions are introduced into the material for optically active centers and the luminescence spectra of Eu^{3+} ions have been measured as a function of excitation wavelength for samples with various Y^{3+} concentrations. The Eu^{3+} ion has a singlet free-ion energy level ($^5D_0$) and generally well-resolved Stark components of $^7F_1$.

These unique spectroscopic characteristics of the Eu^{3+} ion are very useful for experimental study by using site-selective spectroscopy.

II. EXPERIMENT

Transparent polycrystalline samples of CeO_2-Y_2O_3:Eu^{3+} with various Y_2O_3 concentrations were grown by means of a xenon arc imaging furnace. The concentration of Eu^{3+} ions was 0.01 mol %, which were introduced as optical centers in the samples. The concentration of the dopant cation was calibrated by using an x-ray fluorescence analysis. The grown crystals were cut into a rectangular shape and polished to give optical surfaces and used as samples for optical measurements. By using transparent samples, grain-boundary effects of samples on the luminescence spectra can be excluded and the intensity of stray light scattered by the sample is drastically reduced compared with ceramic samples.

The doping effect of the Ln^{3+} ions (e.g., Y^{3+} or Eu^{3+}) on the luminescence center Eu^{3+} in CeO_2 may be twofold: One is a change of Coulomb field which acts on Eu^{3+} ions. The other is the oxygen vacancies, which are introduced in the crystal to compensate the effective negative charge associated with the trivalent dopant. In order to see the influence of the presence of oxygen vacancies on luminescence spectra, samples in which oxygen vacancies are compensated were also investigated. The oxygen vacancies were compensated by adding the same amount of Nb^{5+} ions as Ln^{3+} ions.

Ultraviolet (uv) excitation was achieved by using a Xe lamp. For site-selective spectroscopy measurements, the sample was excited by a pulsed dye laser (rhodamine 6G dye) pumped by a XeCl excimer laser. The tunable output with a spectral width of about 0.04 cm^{-1} was obtained in the 5700–6000-Å wavelength range. This wavelength range corresponds to the wavelength region of the inhomogeneously broadened $^7F_0 - {}^5D_0$ absorption band of Eu^{3+} ions. The samples were mounted into a closed-cycle He refrigerator and cooled down to about 15 K. The luminescence is analyzed with a double-grating monochromator (resolution limit of 1 cm^{-1}) equipped with a photomultiplier and a boxcar integrator.

III. RESULTS

In order to clarify the essential features of the site-selective excitation experiments, we present in Fig. 1 the results of luminescence spectra of 0.4 and 3.8 mol % Y^{3+}-doped CeO_2 samples excited by uv light (2500–3800 Å) from a Xe lamp at 15 K. In this condition all Eu^{3+} ions are excited simultaneously, and in consequence the complicated luminescence spectra which correspond to radiative transitions between $^5D_0$ and ^7F multiplets of Eu^{3+} ions are observed. Although the degeneracy of Stark components of the $^7F_1$ state is three, more than three bands are observed in the wavelength region from 5860 to 5960 Å in this figure. Since this wavelength region corresponds to the $^7F_1$ components, this feature is obviously connected to the existence of different sites of Eu^{3+} ions with different energies for the $^5D_0$-$^7F_1$ transition. The relative intensity of the most intense peak at about 5910 Å decreases and the band width broadens with increasing the dopant concentration. However, the spectral pattern does not essentially change in both samples.

Figure 2 shows the luminescence spectra of the 0.4 mol % Y^{3+}-doped sample under the uv-light excitation (upper part) and the site-selective excitation (lower part). The wavelength of the excitation laser was tuned successively in each peak position of the $^5D_0$-$^7F_0$ luminescence bands for the selective excitation. Distinct luminescence spectra are observed at each excitation wavelength, as seen in the lower part of Fig. 2. Each spectrum excited at different wavelength corresponds to the fluorescence of Eu^{3+} ions at different site. We labeled these sites as A_1, A_2, B, C, and D, which are shown in the figure. The spectral patterns of sites A_1, A_2, and B are essentially the same. Although the upper Stark component of the $^7F_1$ state of the Eu^{3+} ion, which corresponds to the luminescence bands observed at about 5960 Å in Fig. 2, splits into two levels for the site B, the spectral patterns of sites A_1, A_2, and B are qualitatively the same. In

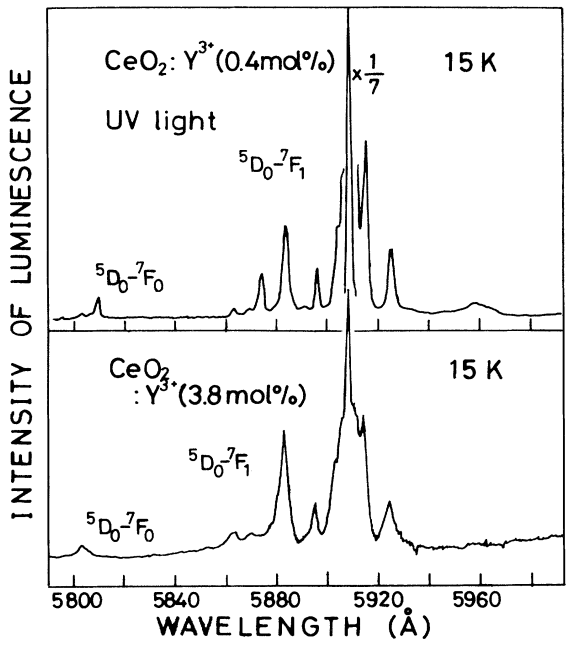

FIG. 1. Luminescence spectra of Eu^{3+} ions excited by uv light at 15 K in 0.4 mol % (upper) and 3.8 mol % (lower) Y^{3+}-doped samples.

contrast to these three sites, the luminescence spectrum of site D is quite different from that of other sites.

The salient feature of these site selective spectra is that a weak luminescence band, which is labeled as "site C," is observed at about 5910 Å in this figure. This weak band is always observed, when the sample is excited by the laser light tuned to the wavelength inside the inhomogeneously broadened $^5D_0$-$^7F_0$ band. This is in contrast to the results under uv-light excitation, where the luminescence band of site C is most intense in the spectrum obtained by the uv-light excitation, as seen in Fig. 2. Furthermore, the radiative life time of site C is several times longer than that of other sites. These results indicate that the Eu^{3+} ion at site C can not be excited via the $^5D_0$-$^7F_0$ absorption band. In other words, the transition probability between these levels is very small for Eu^{3+} ions at site C.

The top spectrum in Figs. 3 and 4 is obtained by uv-light excitation for 3.8 and 4.9 mol % Y^{3+}-doped samples, respectively. From a comparison of the spectra in Figs. 2–4, the observed bandwidth of the Stark components of $^7F_1$ is found to increase with increasing the dopant concentration. This indicates that the degree of disorder of the host lattice increases with increasing dopant concentration. The lower parts in Figs. 3 and 4 show a series of site-selective spectra for the two samples excited by laser light tuned to the wavelength inside the inhomogeneously broadened $^5D_0$-$^7F_0$ luminescence band. The following point should be pointed out as an important feature. Luminescence bands from the ions at sites A_1 and A_2 are not observed in these samples and those from site B become dominant. Instead of the luminescence bands from ions at sites A_1 and A_2, other new bands appear in the spectra, where the peak positions of the new luminescence bands differ from those of sites A_1, A_2, and B. We assign this luminescence band to a different site of Eu^{3+} ions and label this site "site X." The intensity of the luminescence from site X increases with increasing dopant concentration.

As seen in Fig. 4, the splitting energy of the upper Stark components of the $^7F_1$ state of Eu^{3+} ions at site X

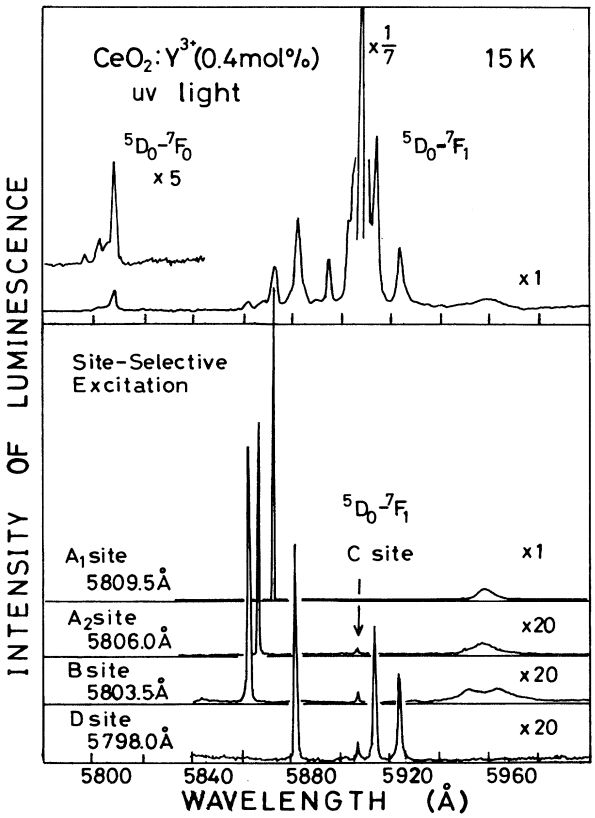

FIG. 2. Luminescence spectra of Eu^{3+} ions measured on the 0.4 mol % Y^{3+}-doped sample. The top spectrum in this figure is excited by uv light. The lower spectra are measured under site-selective excitation, which are excited via the inhomogeneously broadened $^5D_0$-$^7F_0$ absorption band.

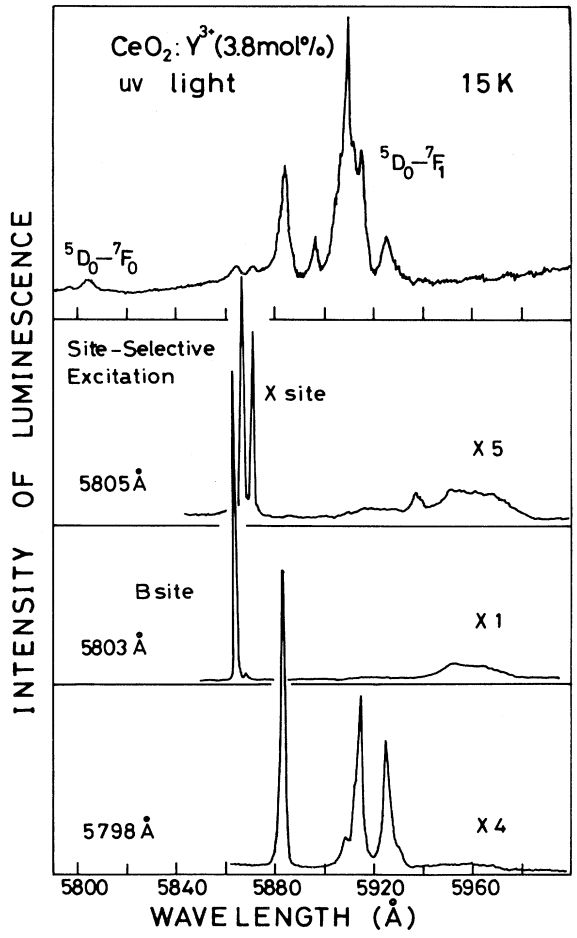

FIG. 3. Luminescence spectra of Eu^{3+} ions measured on the 3.8 mol % Y^{3+}-doped sample. The top spectrum in this figure is excited by uv light. The lower spectra are measured under site-selective excitation, which are excited via the inhomogeneously broadened $^5D_0$-$^7F_0$ absorption band.

is larger than that at site B. This feature is displayed in Fig. 5. In this figure the peak position of each band of sites B and X for the 4.9 mol% Y^{3+}-doped sample is plotted as a function of excitation wavelength. The peak positions of the luminescence bands from $^5D_0$ to the upper Stark level of $^7F_1$ are determined by fitting the spectral line shape to a Gaussian curve. The energy difference of the Stark components of $^7F_1$ and $^5D_0$ continuously shifts to the high-energy side with increasing the excitation photon energy. This result shows that there are many sites of Eu^{3+} ions, which suffer a slightly different crystal field in either case of sites B and X. As seen in this figure, the splitting energy of the upper Stark components of the two sites is different, but the excitation wavelength dependence of the peak position of the luminescence band from site X is quite similar to that

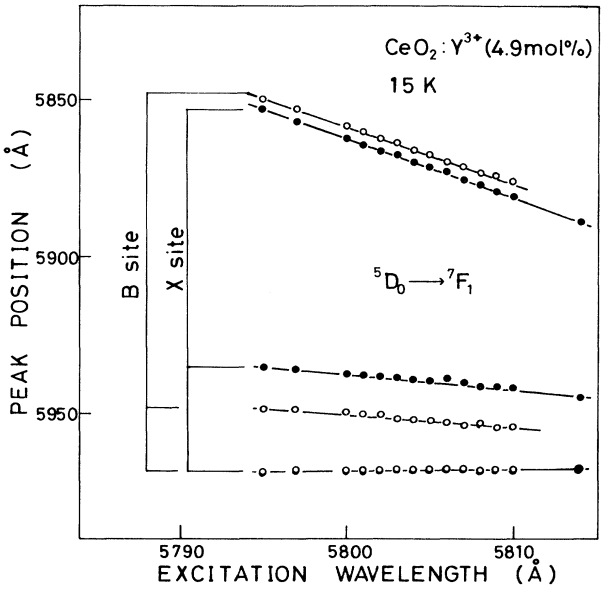

FIG. 5. Peak positions of the luminescence bands of the B and X sites in the 4.9 mol% Y^{3+}-doped sample are plotted against the excitation wavelengths.

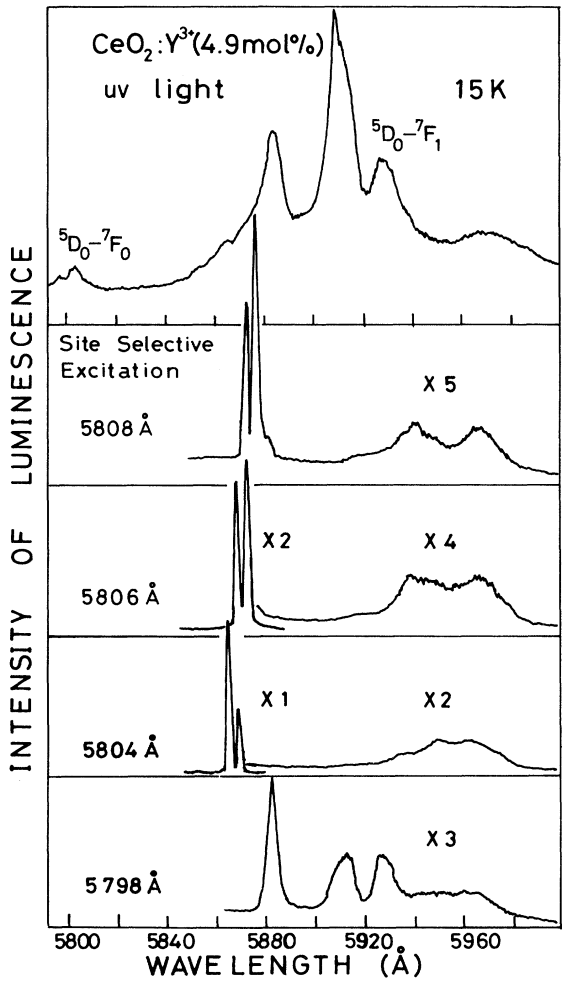

FIG. 4. Luminescence spectra of Eu^{3+} ions measured on the 4.9 mol% Y^{3+}-doped sample. The top spectrum in this figure is excited by uv light. The lower spectra are measured under site-selective excitation, which are excited via the inhomogeneously broadened $^5D_0$-$^7F_0$ absorption band.

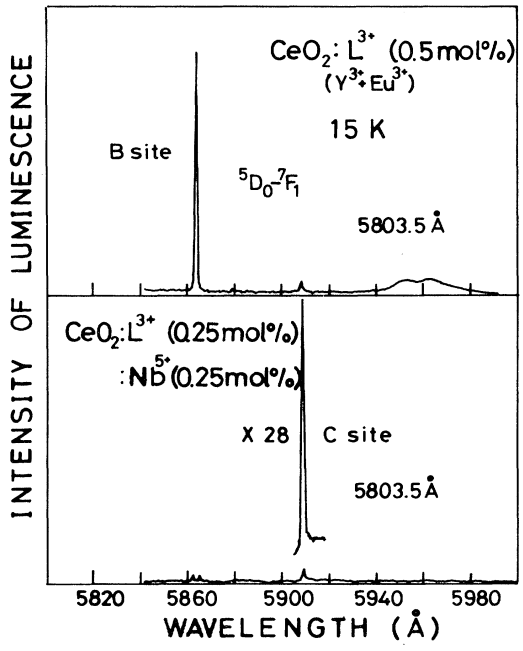

FIG. 6. Luminescence spectra of Eu^{3+} ions measured on two samples. The upper and lower spectra are recorded on V_O introduced and V_O compensated samples, respectively. The total concentrations of impurity metal ions in the two samples are the same, as shown in the figure.

from site B. This result suggests that the configuration of the nearest-neighbor oxygen ions at site X, which is a fundamental structure of the defects in this material, may be similar to that at site B.

Considering the above results shown in Figs. 2–4, we can classify the sites of Eu^{3+} ions into six types, i.e., sites A_1, A_2, B, C, D, and X. To clarify the nature of each site, we measured luminescence spectra on another sample in which oxygen vacancies are compensated by codoping of Nb^{5+} ions. Drastic changes are observed in the site-selective spectra of all measured samples. Except for the case of site C, the intensity of the luminescence bands from sites A_1, A_2, B, D, and X is drastically reduced, when the samples are excited at the wavelength region of the $^5D_0$-$^7F_0$ band. For example, one of the results for the case of site B is shown in Fig. 6. The luminescence band from site B almost disappears, and the band from site C becomes predominant in the sample where the vacancy is compensated. This result strongly indicates that oxygen vacancies closely relate to the local structures at Eu^{3+}-ions sites except for site C. In other words, it is confirmed that only site C is vacancy-free site. These experimental results measured by the vacancy-compensated samples yield conclusive information for a determination of a model for each site.

IV. DISCUSSION

A. Local structures in the dilute range of dopant

In this section we will discuss the nature of each Eu^{3+}-ion site in the dilute range of dopant and make the assignment of the local structures surrounding the trivalent ions.

By using the results of the site-selective spectra, energy diagrams of several excited states, which are measured from the excited state $^5D_0$, for the Eu^{3+} ion of each classified site are shown in Fig. 7 for the 0.2 mol% Y_2O_3-doped sample. The energy of the $^7F_0$ state of Eu^{3+} ions at site C could not be determined from the results of the present study, because neither absorption nor luminescence bands by the transition between $^7F_0$ and $^5D_0$ states were observed. Then the energy of the $^7F_0$ state for site C, which is shown in Fig. 7, is assumed to be equal to that of site D.

The $^7F_1$ state, which is threefold degenerate, is splitting into two or three levels except for site C. The center of gravity and the magnitude of the splitting of the $^7F_1$ state for each of the sites A_1, A_2, and B are almost the same energy. This means that the crystal-field strengths at these three sites are almost the same. This in turn suggests that the fundamental structure of these sites may be similar. The point-group symmetry of the metal-ion site in the fluorite structure crystal is ideally O_h, where the three Stark components of the $^7F_1$ state are degenerate. The above-mentioned results indicate that the point symmetry of the metal ion at sites A_1 and A_2 becomes lower than O_h and only an axial symmetry remains. Considering the results of luminescence measurement on Nb-doped samples, in which the intensity of sites A_1, A_2, and B becomes very weak as shown in Fig. 6, it is reasonable for this system to assign sites A_1 and A_2 to local centers accompanied by an oxygen vacancy at the nearest-neighbor (NN) site, i.e., a (V_O, Eu) cluster. Since the point-group symmetry at these sites is C_{3v}, the experimental results can be well explained. Thus sites A_1 and A_2 can be considered as isolated or quasi-isolated (V_O,Eu) cluster sites, as shown in Fig. 8. This assignment is consistent with results obtained by other methods. For example, the existence of such as the (V_O,Y) cluster has been suggested by dielectric relaxation measurements[9] for the CeO_2-Y_2O_3 system.

The feature of luminescence bands related to the upper Stark levels in these three sites is interesting. The luminescence bands for site A_2 are broader than those for site A_1, and furthermore, the $^7F_1$ level for site B is

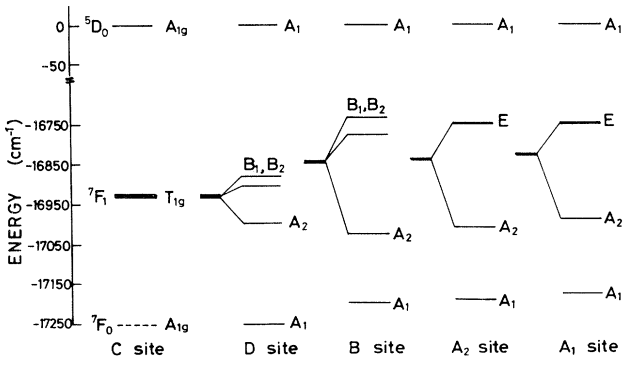

FIG. 7. Energy diagrams of Eu^{3+} ions in the five sites observed in the site-selective spectra in the samples of the dilute range of dopant. The energy of each level is measured from the $^5D_0$ excited state, which is the initial state of luminescence in this study.

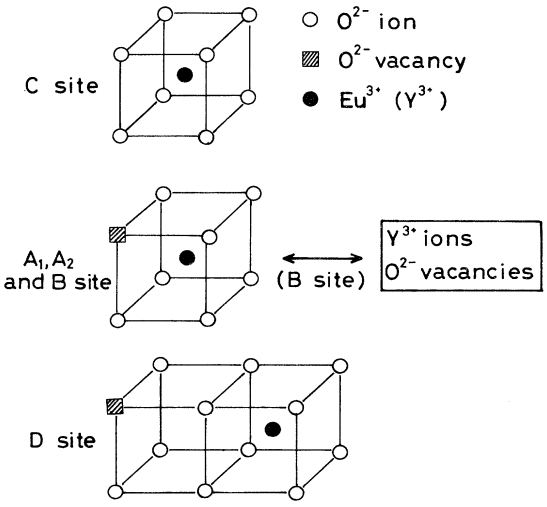

FIG. 8. Local-structure models for the five different sites.

slightly split into two levels. This behavior of the luminescence spectra shows that the point-group symmetry of Eu^{3+}-ion sites becomes lower in order of A_1, A_2, and B, and finally, the local symmetry of site B becomes a distorted C_{3v}. The excitation wavelength dependence of the luminescence peak position of the lower Stark component of $^7F_1$ is shown in Fig. 9(a) for Eu^{3+} ions at sites A_1, A_2, and B. Since the peak position of the luminescence band from the A_1 site continuously changes into that from site A_2 with decreasing the excitation wavelength, the local structure of the A_1 site is essentially the same as that of the A_2 site and only the strength of the crystal field which acts on the two centers is different. On the other hand, the peak position of the luminescence band from the B site is well separated from those from the A_1 and A_2 sites, as seen in Fig. 9 (a). This result suggests that there is a decisive difference in the local structures between site B and the other two sites (A_1 and A_2), although these three defect centers contain the (V_O,Eu) cluster in common. Then we can attribute this difference of local structures to the difference of strength of interaction between the (V_O,Eu) cluster and other defects, i.e., Y^{3+} ions or oxygen vacancies (see Fig. 8).

Now, it is important to determine the kind of defects which interact with the (V_O,Eu) pair at the B site. The possible defects which interact with the (V_O,Eu) pair are free Y^{3+} ions, free oxygen vacancies, and other (V_O,Y) pairs. Since one oxygen vacancy is introduced by doping of two Y^{3+} ions, the probability that a free oxygen vacancy exists near the (V_O,Eu) pair center must be very small in the dilute range of dopant. The number of other free Y^{3+} ions may be almost equal to that of other (V_O,Y) pairs. However, it is difficult to determine that the Y^{3+} ions, which interact with the (V_O,Eu) pair, are free or accompanied by an oxygen vacancy. For these reasons, we assume in this paper that the interacting defects are free Y^{3+} ions.

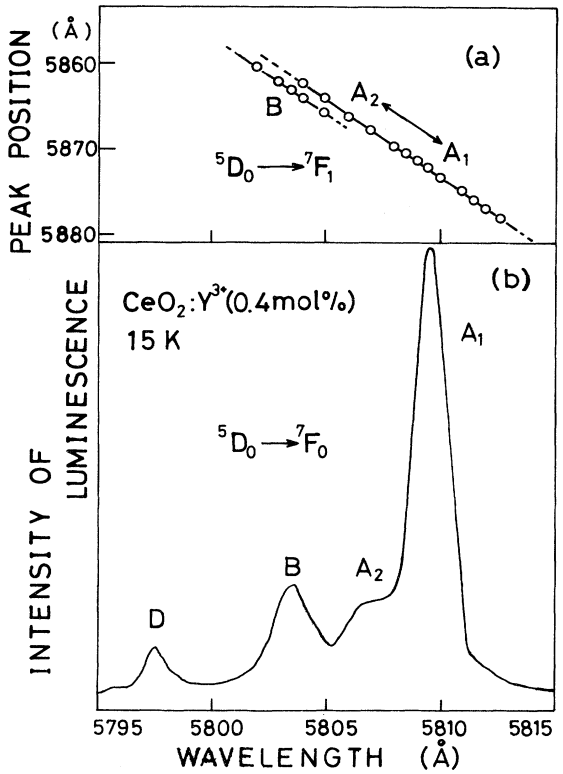

FIG. 9. (a) Peak positions of the lower Stark components of the Eu^{3+} ions at the A_1, A_2, and B sites in the 0.4 mol % Y^{3+}-doped sample are plotted against the excitation wavelengths. (b) Luminescence spectra corresponding to the $^5D_0$-$^7F_0$ transition of the Eu^{3+} ion.

Luminescence properties of Eu^{3+} ions at site C are quite different from those at other sites in several respects. At first, the luminescence band from Eu^{3+} ions at site C is strongly excited only by uv light and is not clearly observed under the site-selective excitation condition. This fact indicates that the transition probability between $^7F_0$ and $^5D_0$ is very small. Since this transition has the nature of the electric dipole transition, it is possible to explain this experimental fact if site C has an inversion symmetry. Second, since only one band is observed in the spectra for site C, as seen in Fig. 2, it is concluded that the Stark components of the $^7F_1$ of Eu^{3+} ions at this site are all degenerate. This degeneracy of the $^7F_1$ state is consistent with the result of symmetry consideration for site C. As shown in Fig. 6, it is the most significant and characteristic feature of the luminescence from site C ions that the intensity of luminescence is not quenched by the codoping of Nb^{5+}, in other words, by the compensation of oxygen vacancies. These experimental results indicate that site C is a local center without oxygen vacancies. Therefore, it is most reasonable to assign C site to the normal Ce-ion site in the fluorite structure as show in Fig. 8, where the point-group symmetry of the metal ion is O_h.

For the D site, the energy of the center of gravity and the splitting of the $^7F_1$ state are different from those of sites A_1, A_2, and B. Since the upper Stark level clearly splits for site D, as shown in Fig. 2, the local symmetry of site D is C_{2v} or lower. Since the energy difference between the $^5D_0$ state and the center of gravity of the $^7F_1$ state of Eu^{3+} ions at site D is almost the same as that at site C, which has O_h symmetry in the above discussion, the strength of the local crystal field which acts on ions at site D does not much deviate from that for metal sites in the fluorite structure. Luminescence intensity from site D is very weak for the Nb^{5+}-doped sample. This result suggests that the local structure of site D is closely related to oxygen vacancies. Considering these results for site D, we propose a model for the local structure of site D, as shown in Fig. 8. In this model, the NN configuration of the Eu^{3+} ion of site D is the same as that of the fluorite structure; i.e., there is no oxygen vacancy in the NN site, and an oxygen vacancy exists at the 2NN or the 3NN oxygen sites, etc. The position of the oxygen vacancy is not clear at present.

B. Relationship between the defect structures and the ionic conductivity

In this section we will discuss the dopant-concentration dependence of the site-selective spectra

and clarify the relationship between the local structures of defects and the ionic conductivity in this system. Especially, we want to reveal the effect of the interaction between impurity metal ions and oxygen vacancies on the ionic conduction. For this purpose, it is most useful to focus our attention on the (V_O,Y) cluster sites, i.e., A_1, A_2, B, and X sites, in this material.

Excitation spectra for several samples with different dopant concentrations have been measured in order to discuss the intensity variation of the luminescence from each (V_O,Y) cluster site as a function of the dopant concentrations. The results for five samples are shown in Figs. 10 and 11. It is the most evident feature in Fig. 10 that the luminescence intensity from site A_1 decreases drastically with increasing the dopant concentration. This behavior is quite consistent with the previously introduced defect structure model, in which the site A_1 is an isolated (V_O,Y) cluster. With increasing the dopant concentration, on the other hand, the luminescence intensity from site B becomes dominant and that from site X also grows up.

In order to estimate the relative luminescence intensity of each site, the integrated area of excitation spectrum is calculated for each site as the total intensity of luminescence of each site. In this procedure the total area of the excitation spectrum in each sample is normalized to unity.

Assuming that the relative intensity of the luminescence from the different (V_O,Eu) sites is in proportion to the existence ratio of these sites, we have estimated the existence ratio of these sites from the relative intensity of luminescence among sites A_1, A_2, B, and X. This assumption is not always correct in luminescence studies, because the quantum efficiency of the luminescence of Eu^{3+} ions in each site may be different from each other. In this case, however, the type of local structures of the sites are all the same essentially; i.e., all sites contain the (V_O,Eu) pair. Then the quantum efficiencies of absorption and luminescence at all sites may be expected to be comparable to each other. For this reason we think that the assumption holds in this case.

The dopant-concentration dependence of the existence ratio $\rho(I)$ of site I (I: A_1, A_2, B and X) is shown in Fig. 12 (b) with several marks. From this figure the sites of Eu^{3+} ions in Y^{3+}-doped CeO_2 crystal can be classified into three categories: (1) A_1 and A_2 sites, which show a monotonic decrease of existence ratio with increasing dopant concentration; (2) B site, which shows a max-

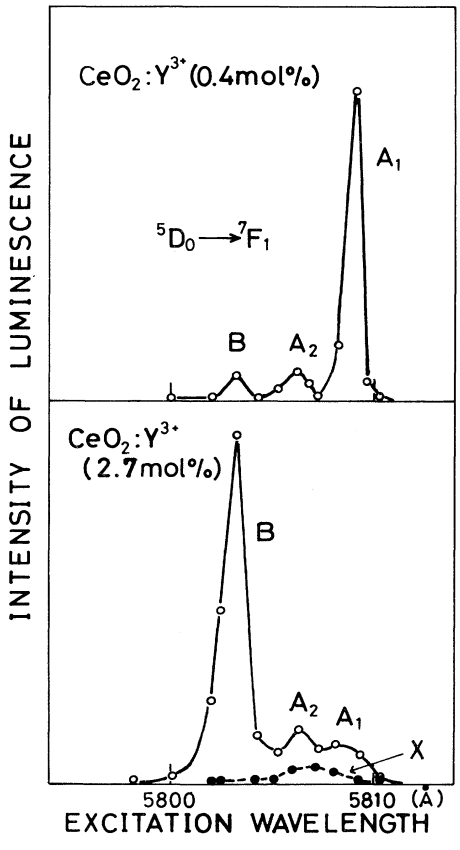

FIG. 10. Excitation spectra for the lower Stark component of the $^5D_0$-$^7F_1$ luminescence bands measured on the 0.4 mol % (upper) and 2.7 mol % (lower) doped samples.

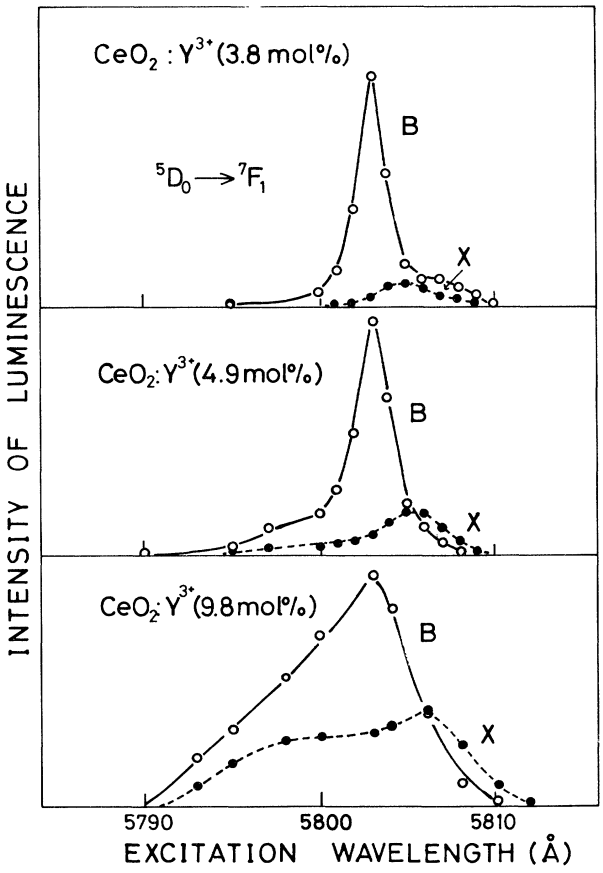

FIG. 11. Excitation spectra for the lower Stark component of the $^5D_0$-$^7F_1$ luminescence bands measured on three different samples with different dopant concentrations.

imum of existence ratio at about 3 mol % Y_2O_3; and (3) X site, which shows a monotonic increase of existence ratio with increasing dopant concentration. The A_1 and A_2 sites are an isolated or quasi-isolated (V_O,Eu) cluster, as described in the previous section. Then the behavior of category (1) seems to be quite reasonable, because the number of isolated sites should decrease in the high doping region. In contrast to A_1 and A_2 sites, the X site is considered to be the (V_O,Eu) pair site which is strongly perturbed by other defects. So the rapid increase of $\rho(X)$ indicates that the interaction between local defects becomes strong at higher dopant concentrations, especially above 4 mol % Y_2O_3.

It is interesting to compare the dopant-concentration dependence of $\rho(B)$ and $\rho(X)$ with that of the ionic conductivity. The maximum of $\rho(B)$ is observed at about 3 mol % Y_2O_3, which corresponds to the dopant concentration for the conductivity maximum[8] as seen from Fig. 12(a). Furthermore, it should be noted that the rapid increase of $\rho(X)$ and the rapid decrease of $\rho(B)$ above 4 mol % seem to be closely related with the rapid increase of the activation energy for the ionic conduction leading to the rapid decrease of the ionic conductivity. These results suggest that sites B and X may be closely related to the ion conducting mechanism. In other words, the defect interactions between the (V_O,Eu) cluster and Y^{3+} defect play an important role in the ionic conduction mechanism of this material.

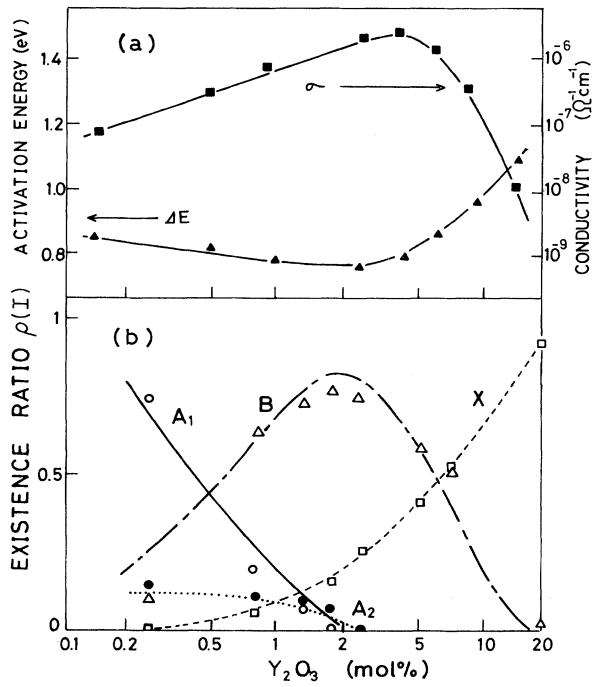

FIG. 12. (a) Dopant-concentration dependence of the ionic conductivity and activation energy of this system reported by Wang *et al.* (Ref. 8). (b) The dopant-concentration dependence of the existence ratio of the four (V_O,Eu) cluster sites. The dashed line is drawn as a guide to the eye. Other lines represent the dopant-concentration dependence of the calculated existence ratio of the sites.

We think that the defect interaction between the (V_O,Eu) cluster and Y^{3+} defects must closely relate to the distance between them. So we have tried to evaluate the distance between the (V_O,Eu) cluster and Y^{3+} defects from the dopant-concentration dependence of $\rho(I)$ (I: A_1, A_2, and B), in order to clarify a more microscopic picture of the defect structure and defect interaction in each site. In this procedure we calculate the dopant-concentration dependence of the existence ratio of (V_O,Eu) clusters having Y^{3+} defects at different distances, assuming that the Y^{3+} defects randomly distribute in crystal. Comparing the calculated results with experimentally obtained ones, we determine the most plausible defect structure, i.e., the distance between the (V_O,Eu) cluster and a Y^{3+} defect in each of the sites A_1, A_2, and B.

The dopant-concentration dependence of the calculated existence ratio of several different defects is shown in Fig. 12(b) by using several different kinds of lines, which most well reproduce the dopant-concentration dependence of $\rho(I)$ (I: A_1, A_2, and B). The solid line in this figure represents the calculated existence ratio of a defect, which is a given (V_O,Eu) pair having no Y^{3+} ions in the volume confined within the 6NN cation sites. Since site A_1 is assigned to an isolated (V_O,Eu) cluster defect, it can be said that the distance between the Eu^{3+} ion and the 6NN is a critical one which causes no interaction between the (V_O,Eu) pair and a Y^{3+} ion in this material. The dotted line represents the dopant-concentration dependence of the calculated existence ratio of a defect, which is a given (V_O,Eu) pair having one Y^{3+} ion at one of the 5NN cation sites. The dot-dashed line represents the dopant-concentration dependence of the calculated existence ratio of a given (V_O,Eu) defect, which is calculated by assuming less than five Y^{3+} ions in the region confined within the 4NN cation sites, which consist of 54 cation sites.

The $^7F_1$ state of the Eu^{3+} ion at site B splits into three Stark components. This face suggests that the interaction between the (V_O,Eu) pair and Y^{3+} ions at site B is strong enough to change the C_{3v} symmetry at this site into a lower one. The evidence of such a strong interaction between the (V_O,Y) pair and Y^{3+} is not observed in the luminescence from sites A_1 and A_2, where the upper Stark components are degenerate. This result indicates that the distance between the 4NN ions and Eu^{3+} ion is the critical one for the beginning of the interaction between the Eu^{3+} ion and the other defect.

The dopant-concentration dependence of the existence ratio of site X cannot be fitted by the simple defect model as used in the above discussion. Therefore, the dashed line in Fig. 12(b) is drawn as a guide to the eye. The local structure of site X may be more complex, which is defect clusters having several dopant ions and oxygen vacancies. However, it should be mentioned here that the peak wavelength variation of the luminescence from site X on the excitation wavelength is similar with that from site X as seen in Fig. 5. This similarity strongly suggests that

the basic structure of all defects may be the same; i.e., the main structure in all defects is a (V_O,Eu)-type cluster, while the local structure of the site X is more complex than that of other sites.

In the above discussion, we consider that only Y^{3+} defects interact with the (V_O,Eu) cluster and the influence of other V_O defects is neglected in the dilute range of dopant. This assumption should be verified, if possible, by other experimental methods.

Now, we consider the relationship between the defect interaction and the ionic conductivity in this material. The activation energy of ionic conduction decreases with increasing dopant concentration and shows a minimum at about 4 mol% Y_2O_3. In the region below 4 mol% Y_2O_3, the decrease of $\rho(A_1)$ and $\rho(A_2)$ and the increase of $\rho(B)$ are observed. This result indicates that the interaction between an isolated (V_O,Eu) pair and a Y^{3+} ion rapidly grows up with increasing the dopant concentration in this region. We discuss the influence of this interaction on the ionic diffusion by using the schematic model shown in Fig. 13. Let a (V_O,Eu) or (V_O,Y) pair placed at the center in this figure interact with Y^{3+} ions located in cation sites within the critical distance, which is defined as the distance for beginning of the interaction between the (V_O,Eu) pair and the Y^{3+} ions. Then the inside of a solid circle is the interaction space in this figure. Increasing the dopant concentration, the mean distance between dopant ions will become short and, at last, shorter than the critical distance. If a vacancy associated with an Y^{3+} ion migrates under this situation, the completely free V_O never exists, since the Y^{3+} ions located inside the critical distance always exist around the V_O. This causes a decrease of the association energy and, in consequence, the decrease of the activation energy for ionic conduction which is the sum of the association and migration energies in this diffusion process.

The decrease of activation energy in a dilute region of dopant was observed for the first time by Wang *et al.*[8] with an electrical measurement method. They ensured that the decrease of activation energy is due to an electrostatic interaction between the (V_O,Y) pair and Y^{3+} ions. The present result is consistent with their proposed mechanism.

From the above discussion, it is found that the optimum mean distance between dopant ions exists, where the activation energy will become the minimum value leading to the maximum value of conductivity. At the same time, the existence ratio of site B gives the maximum. Increasing the dopant concentration, the mean distance between them becomes shorter than the critical distance shown in Fig. 13, and finally, for a very high dopant concentration, more than one Y^{3+} ion or oxygen vacancy will interact with the (V_O,Y) pair. This situation causes the increase of activation energy and the decrease of ionic conductivity and, furthermore, the rapid increase of the existence ratio of site X. The complex defect interaction in higher dopant concentration must be investigated by future experiments.

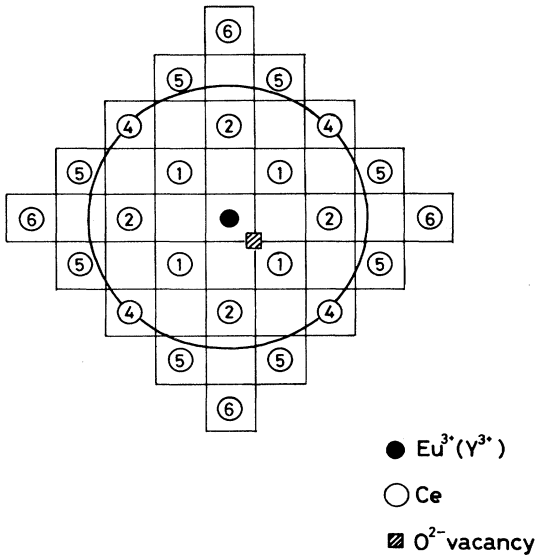

FIG. 13. Schematic crystal structure of CeO_2. The solid straight lines represent the oxygen sublattice and oxygen vacancies exist at the cross points of the two lines. The number I in the open circles represents the Ith NN ion site. The large solid circle represents the critical distance from the Eu^{3+} ion (detailed discussion is given in the text).

V. CONCLUSION

Site-selective spectroscopy has been applied to a superionic conducting system, rare-earth-doped CeO_2. Six different sites of the Eu^{3+} ion are classified, and models of the local structure around these defects are proposed. The existence ratio of different sites is estimated from the dopant-concentration dependence of luminescence intensity. This analysis reveals that the (V_O,Y) pair plays an important role for the ionic conduction in this system. Furthermore, it was made clear in this study that the dopant-concentration dependence of the conductivity and the activation energy can be explained essentially by considering the interaction between the (V_O,Y) pair and other defects in the region from 0.2 to 20 mol% Y_2O_3.

[1]R. M. Dell and A. Hooper, in *Solid Electrolytes*, edited by P. Hagenmullar and W. van Gool (Academic, New York, 1987), p. 291.

[2]W. L. Worrell, in *Solid Electrolytes*, edited by S. Geller (Springer, Berlin, 1977), p. 143.

[3]T. Takahashi, H. Iwahara, and Y. Nagai, J. Appl. Electrochem. **2**, 97 (1972).

[4]D. Steele and B. E. F. Fender, J. Phys. C **7**, 1 (1974).

[5]S. Suzuki, M. Tanaka, and M. Ishigame, Jpn. J. Appl. Phys. **24**, 401 (1985).

[6]J. B. Cohen, M. Morinaga, and J. Faber, Jr., Solid State Ionics **3/4**, 61 (1981).

[7]S. Hull, T. W. D. Farley, M. A. Hackett, W. Hayes, R. Osborn, N. H. Andersen, K. Clausen, M. T. Hutchings, and W. G. Stirling, Solid State Ionics **28-30**, 488 (1988).
[8]D. A. Wang, D. S. Park, J. Griffith, and A. S. Nowick, Solid State Ionics **2**, 95 (1981).
[9]D. A. Wang and A. S. Nowick, J. Phys. Chem. Solids **44**, 639 (1983).
[10]B. E. F. Fender, in *Chemical Applications of Thermal Neutron Scattering,* edited by B. T. M. Willis (Oxford University Press, London, 1973), p. 250.
[11]M. P. Anderson, D. E. Cox, K. Halperin, and A. S. Nowick, Solid State Ionics **9/10**, 953 (1983).
[12]C. Brecher and L. A. Riseberg, Phys. Rev. B **13**, 81 (1976).
[13]R. C. Linares, J. Opt. Soc. Am. **56**, 1700 (1966).